ECCOMAS Congress 2016
VII European Congress on Computational Methods in Applied Sciences and Engineering
M. Papadrakakis, V. Papadopoulos, G. Stefanou, V. Plevris (eds.)
Crete Island, Greece, 5–10 June 2016

ADVANCES IN THE BOUNDARY ELEMENT METHOD IN GEOMECHANICS

Gernot Beer[1,2]

[1]emeritus Professor
Institute for structural analysis
University of Technology, Graz, Austria
e-mail: gernot.beer@tugraz.at

[2] conjoint Professor
ARC Centre of Excellence for Geotechnical Science and Engineering
The University of Newcastle, Australia

Keywords: Boundary Element Method, geomechanics.

Abstract. *In this work a novel approach is presented for the Boundary Element analysis of problems in geomechanics. Firstly, Non-Uniform Rational B-Spines (NURBS) are used for the description of the geometry and for the approximation of the unknowns. This results in a significant decrease in the number of parameters used for an accurate description of the geometry as well as a decrease in the number of degrees of freedom required for good quality results. Secondly, NURBS are also used for the description of the geometry of geological inclusions, which can have properties different to the rock mass and can experience inelastic behavior.*

After a short introduction to the theory, some details of implementation are shown. On test examples, involving elastic homogeneous domains, it is first shown that the method delivers accurate results with fewer parameters and number of unknowns as compared with conventional analysis. Solutions are compared to either known solutions or with conventional BEM analyses. Geological inclusions are introduced next and results of test examples are compared with Finite Element analyses. Finally a practical example is shown.

1 INTRODUCTION

The Boundary Element Method (BEM) is ideally suited for the analysis of problems in geomechanics as it can easily consider infinite and semi-infinite domains because the radiation condition is implicitly fulfilled. In the case of elastic, homogeneous domains only boundary integrals appear, and the solution involves a discretization of the boundary, thereby reducing the analysis effort by an order of magnitude.

However, to analyze real problems in geomechanics the consideration of heterogeneous and inelastic ground conditions is essential. The BEM can be extended to analyze these problems, but additional volume integrals appear. The numerical solution of the integral equations requires the discretization of a volume, therefore partially destroying the attractiveness of the method. However, the volume integrals only cover the part of the domain that has different material properties or behaves in an inelastic way. Currently the most popular method is to use internal cells for the volume discretization. Cells are like Finite Elements but the main difference is that their only purpose is the evaluation of the volume integral. This means that no additional degrees of freedom are introduced. The requirement for an additional volume discretization seems to have severely restricted the application of the BEM in geomechanics, with the Finite Element or similar domain methods dominating. In this paper it will be shown how piecewise heterogeneous, inelastic domains can be analyzed without a volume discretization, thereby enhancing the applicability of the method for problems in geomechanics.

Isogeometric analysis [1] has gained significant popularity in the last decade because of the fact that geometry data can be taken directly from Computer Aided Design (CAD) programs, potentially eliminating the need for mesh generation. NURBS basis functions, that are used for the definition of the geometry, are able to describe certain geometries such as arcs exactly. Therefore, as will be shown, the number of parameters, required to accurately define geometry, can be reduced significantly. NURBS are also used to define geological inclusions, eliminating the need for a volume discretization.

2 THE BEM WITH VOLUME EFFECTS

To apply the BEM to heterogeneous and inelastic problems, so called body force effects have to be included. Using the theorem of Betti as explained in [2], the boundary integral equation with body forces acting in a sub-volume V_0 can be written in incremental form and in matrix notation as (see Figure 1):

$$\begin{aligned} \mathbf{c}\,\dot{\mathbf{u}}(\mathbf{y}) = &\int_S \mathbf{U}(\mathbf{y},\mathbf{x})\dot{\mathbf{t}}(\mathbf{x})\,\mathrm{d}S + \int_{S_0} \mathbf{U}(\mathbf{y},\bar{\mathbf{x}})\dot{\mathbf{t}}_0(\bar{\mathbf{x}})\,\mathrm{d}S_0 \\ &- \int_S \mathbf{T}(\mathbf{y},\mathbf{x})\dot{\mathbf{u}}(\mathbf{x})\,\mathrm{d}S + \int_{V_0} \mathbf{U}(\mathbf{y},\bar{\mathbf{x}})\dot{\mathbf{b}}_0(\mathbf{x})\,\mathrm{d}V_0 \end{aligned} \tag{1}$$

where $\mathbf{c}$ is a free term, $\mathbf{U}(\mathbf{y},\mathbf{x})$ and $\mathbf{T}(\mathbf{y},\mathbf{x})$ are matrices containing fundamental solutions (Kernels) for the displacements and tractions at a point $\mathbf{x}$ due to a unit force at a point $\mathbf{y}$ [3], $\dot{\mathbf{u}}(\mathbf{x})$ and $\dot{\mathbf{t}}(\mathbf{x})$ are increments of the displacement and traction vectors on the surface S, defining the problem domain. $\dot{\mathbf{b}}_0(\bar{\mathbf{x}})$ are increments of body force inside the inclusion and $\dot{\mathbf{t}}_0(\bar{\mathbf{x}})$ are increments of tractions related to the body force acting on surface S_0 bounding V_0.

The integral equations can be solved for the unknowns $\mathbf{u}$ or $\mathbf{t}$ by discretization. As in the majority of previous work on the isogeometric BEM [4, 5, 6, 7, 8, 9, 10] we use the collocation method, i.e. we write the integral equations for a finite number, N, of source or collocation

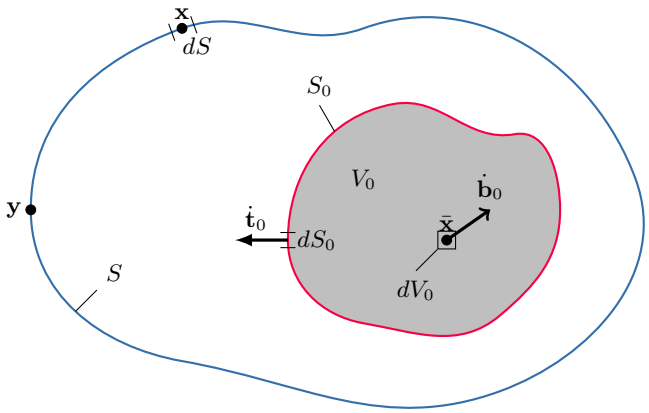

Figure 1: Explanation of the derivation of the integral equation with volume effects

points $\mathbf{y}_n$:

$$\mathbf{c}\,\dot{\mathbf{u}}\,(\mathbf{y}_n) = \int_S \mathbf{U}\,(\mathbf{y}_n,\mathbf{x})\,\dot{\mathbf{t}}\,(\mathbf{x})\,\mathrm{d}\,S + \int_{S_0} \mathbf{U}\,(\mathbf{y}_n,\bar{\mathbf{x}})\,\dot{\mathbf{t}}_0\,(\bar{\mathbf{x}})\,\mathrm{d}\,S_0 \tag{2}$$
$$- \int_S \mathbf{T}\,(\mathbf{y}_n,\mathbf{x})\,\dot{\mathbf{u}}\,(\mathbf{x})\,\mathrm{d}\,S + \int_{V_0} \mathbf{U}\,(\mathbf{y}_n,\bar{\mathbf{x}})\,\dot{\mathbf{b}}_0\,(\bar{\mathbf{x}})\,\mathrm{d}\,V_0$$

with $n = \{1,\ldots,N\}$.

For the numerical evaluation of the surface integrals over S we divide the boundary into patches and use a geometry independent field approximation approach for each patch, i.e. we use different basis functions for the description of the geometry and for the field values:

$$\mathbf{x}^e = \sum_{k=1}^{K} N_k(\mathrm{u}) \cdot \mathbf{x}_k^e \tag{3}$$

$$\mathbf{u}^e = \sum_{k=1}^{K^d} N_k^d(\mathrm{u}) \cdot \mathbf{u}_k^e \tag{4}$$

$$\mathbf{t}^e = \sum_{k=1}^{K^t} N_k^t(\mathrm{u}) \cdot \mathbf{t}_k^e \tag{5}$$

In the above the superscript e refers to the number of the patch, N_k,N_k^d, N_k^t are NURBS basis functions of the local coordinate u for describing the geometry $\mathbf{x}^e$, displacements $\mathbf{u}^e$ and tractions $\mathbf{t}^e$, $\mathbf{x}_k^e$ specify the location of control points, $\mathbf{u}_k^e$,$\mathbf{t}_k^e$ are parameter values and K, K^d, K^t specify the number of parameters for each patch.

For an excavation problem for example the following system of equations can be assembled:

$$[\mathbf{T}]\,\{\mathbf{u}\} = \{\mathbf{F}\} + \{\mathbf{F}\}_0 \tag{6}$$

where $[\mathbf{T}]$ is an assembled matrix with coefficients related to Kernel $\mathbf{T}$ and $\{\mathbf{u}\}$ is a vector that collects all displacement components on points $\mathbf{y}_n$. $\{\mathbf{F}\}$ is a vector related to the the applied excavation tractions and $\{\mathbf{F}\}_0 = \{\mathbf{F}\}_0^{S_0} + \{\mathbf{F}\}_0^{V_0}$ is the right hand side related to the body force effects, i.e. related to the integrals over S_0 and V_0 in Equation (2). Details of the implementation of the isogeometric BEM for elastic homogeneous domains can be found in [3, 11].

3 NURBS basis functions

An detailed treatise on NURBS basis functions is presented in [3], here only a short explanation is given. NURBS or Non-uniform rational B-splines are an extension of classical B-splines. To define B-splines we start with a *knot vector*. This is a vector containing a series of non-decreasing values of the local coordinate:

$$\Xi = \begin{pmatrix} \mathrm{u}_0 & \mathrm{u}_1 & \cdots & \mathrm{u}_N \end{pmatrix} \tag{7}$$

We define the entries in the vector as *knots*. With the knot vector a recursive formula is applied. First we compute the functions for order $p = 0$ (constant) and for $i = 0, \cdots, N$.

$$N_{i,0}(\mathrm{u}) = \begin{cases} 1 & \text{if} \quad \mathrm{u}_i \leqslant \mathrm{u} < \mathrm{u}_{i+1} \\ 0 & \text{otherwise} \end{cases} \tag{8}$$

Higher order basis functions are defined by referencing lower order functions:

$$N_{i,p}(\mathrm{u}) = \frac{\mathrm{u} - \mathrm{u}_i}{\mathrm{u}_{i+p} - \mathrm{u}_i} N_{i,p-1}(\mathrm{u}) + \frac{\mathrm{u}_{i+p+1} - \mathrm{u}}{\mathrm{u}_{i+p+1} - \mathrm{u}_{i+1}} N_{i+1,p-1}(\mathrm{u}) \tag{9}$$

NURBS basis functions are obtained by including weights, w_i :

$$R_{i,p}(\mathrm{u}) = \frac{N_{i,p}(\mathrm{u})\,\mathrm{w}_i}{\sum_{j=0}^{I} N_{j,p}(\mathrm{u})\,\mathrm{w}_j} \tag{10}$$

4 Geometry description with NURBS

NURBS are ideally suited for the description of geometry (for example they are able to describe circular arcs exactly) and this is one of the main reasons they are used by the CAD community. The main difference to commonly used Lagrange polynomials, is that the concept of nodal points is replaced by a concept of control points, which do not always lie on the curve.

As an example we show the description of the geometry of an NATM tunnel, where the design shape is specified by arcs (center, radius and extent) as shown in the tables in Figure 2. One half of the tunnel can be described with 1 NURBS patch of order 2 and only 7 control points.

This describes exactly the design geometry. It is noted that some control points do not lie on the curve. The control polygon that connects the control points indicates that there is a smooth transition (unique tangent) between the arcs.

5 Approximation of unknowns with NURBS or B-splines

NURBS or B-spline basis functions are also ideally suited for the approximation of the unknown. In contrast to the commonly used Lagrange polynomials they offer more advanced refinement features. The main difference is that basis functions are not linked to nodal points, but to anchors.

The continuity of B-splines can be controlled by the knot vector. Knots that are repeated at the beginning and the end, control the order of the function. For example knot vectors $\Xi = (0,0,0,1,1,1)$ and $\Xi = (0,0,0,0,1,1,1,1)$ result in basis functions of order 2 and 3 respectively as shown in Figure 3.

In Figure 4 we show how the extent and continuity of the basis functions can also be controlled by the knot vector. In the left we see that the first and last basis function has a limited

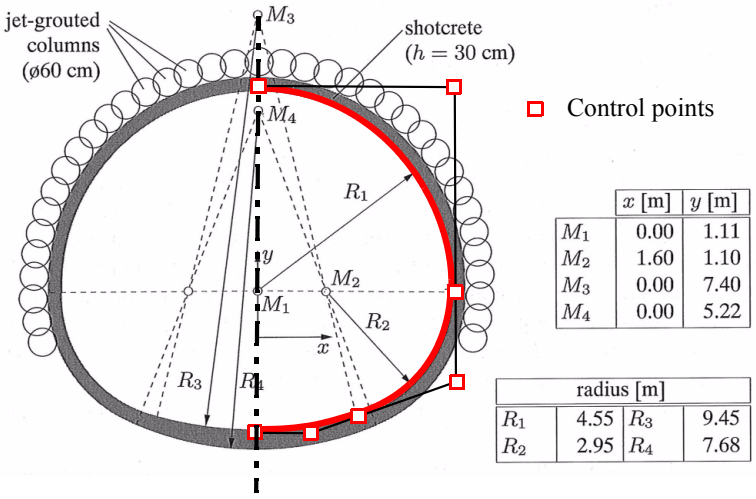

	x [m]	y [m]
M_1	0.00	1.11
M_2	1.60	1.10
M_3	0.00	7.40
M_4	0.00	5.22

radius [m]			
R_1	4.55	R_3	9.45
R_2	2.95	R_4	7.68

Figure 2: Example of geometry description with NURBS: NATM Tunnel definition, description of right half with NURBS basis functions, showing control points and control polygon.

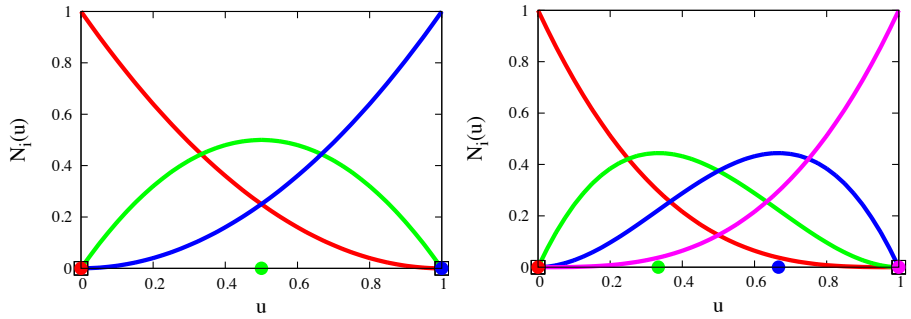

Figure 3: Example of order elevation: Left, B-splines of order 2 and right of order 3. Knot locations are depicted by squares, anchors by filled circles

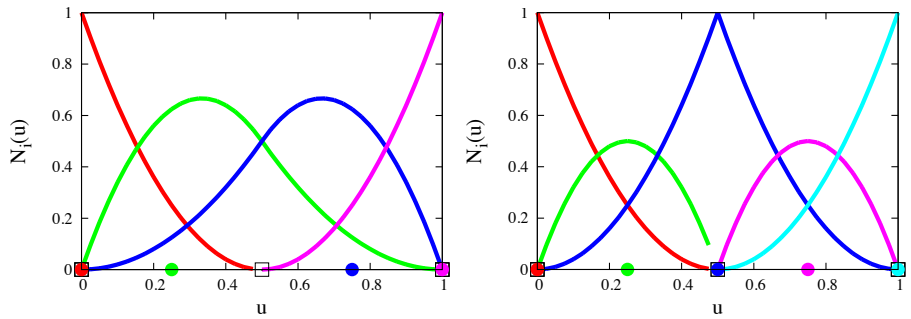

Figure 4: Example of knot insertion: B-splines of order 2 with (left) $\Xi = (0,0,0,0.5,1,1,1)$ and (right) $\Xi = (0,0,0,0.5,0.5,1,1,1)$.

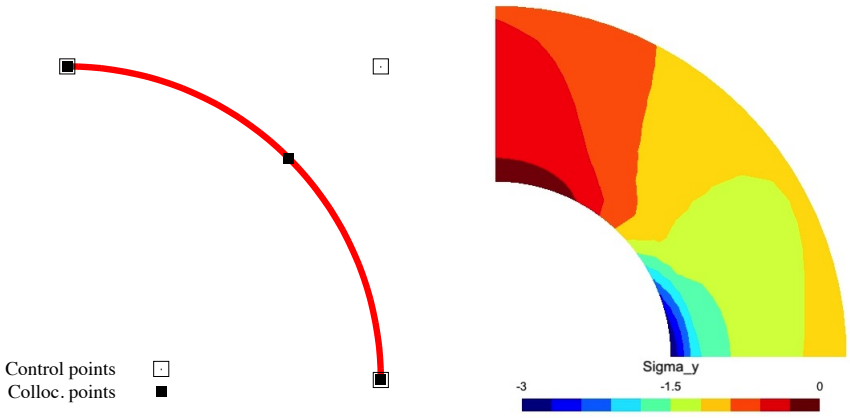

Figure 5: Test example circular excavation: Left definition of a quarter of a circle with one NURBS curve and right resulting stress distribution

span, i.e. span only half the parameter space, whereas in the right we can see that the basis functions are discontinuous at u=0.5.

This means that refinement strategies are simply implemented by changing the knot vector and this is in contrast to isoparametric elements, that involves a change of element type (to higher order) or an increase in the number of elements. The classical p-refinement can be achieved by increasing the number of repetitions at the beginning and end of the knot vector, whereas a refinement similar to the classical h-refinement can be achieved by inserting values into the knot vector. For basis functions of oder 2, for example, inserting one value means that the basis functions have limited span but are still continuous. Repetition of the inserted value means that the basis functions are discontinuous. This refinement strategy would be identical to a classical h-refinement.

In the following we show first examples involving a homogeneous, elastic domain and then consider geological inclusions.

6 Test example

This example is designed to demonstrate how very accurate (or in this case exact) results can be obtained with a very coarse discretization. It relates to the simulation of a circular excavation in an elastic prestressed domain. The following data describes the problem:

E=10; Poissons ratio=0.3, virgin stress $\sigma_{x0} = 0$, $\sigma_{y0} = -1$.

The exact solution of this problem is known. Only one quarter of the problem was analyzed with two axes of symmetry assumed. The geometry is described by one NURBS patch defined with a basis function of order 2 and 3 control points. This exactly describes a quarter circle. The same basis function as for the description of the geometry was used (isogeometric approach) resulting in the collocation points shown in the left of Figure 5. This means that the mesh has only 6 degrees of freedom. The exact solution for the stress concentration is 3.0. As can be seen on the right of Figure 5 the simulation yields the exact solution in this case.

7 Practical example

Here we present an example of the analysis of an NATM tunnel. The geometry of the tunnel is defined by arcs as shown in Figure 2. The tunnel is excavated in a homogeneous elastic domain with the following properties: $E = 10000\,MPa, \nu = 0.3$. The virgin stress field was

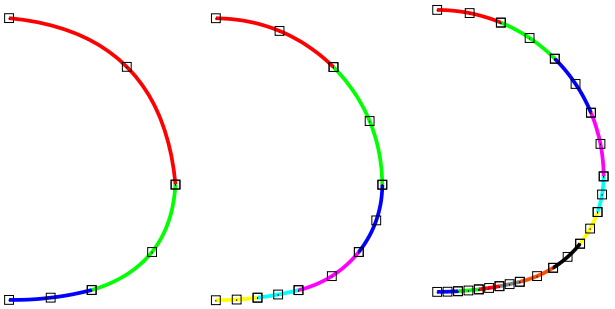

Figure 6: Approximation of geometry of half the tunnel with conventional BEM and a classical h-refinement (Elements are color coded). Nodal points are depicted by hollow squares. Note that the approximation of the geometry changes (i.e. improves) with refinement.

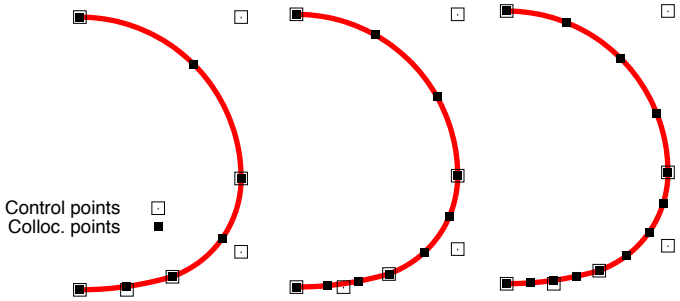

Figure 7: Definition of geometry of half the tunnel using one NURBS patch of order 2. Refinement of solution by order elevation showing collocation points (from left to right oder 2 to 4). Collocation points are depicted by filled squares. Note that in contrast to the above the description of the geometry (already exact) does not change.

assumed to be $\sigma_{x0} = -0.4, \sigma_{y0} = -1.0\,MPa$. We show the salient differences between a conventional and a NURBS based analysis by comparing the two.

7.1 Conventional BEM analysis

In the conventional BEM analysis Lagrange polynomials are used for the approximation of the geometry and the unknown (= isoparametric boundary elements). A refinement of the solution can be obtained either by increasing the order of the element (p-refinement), or by increasing the number of elements (h-refinement). In most cases h-refinement is used. Figure 6 shows the approximation of the geometry of half of the tunnel and of the unknowns by increasing the number of elements. We see that for this refinement strategy both a better approximation of the geometry as well of the unknown is achieved.

7.2 NURBS based approach

Here half of the tunnel is discretized with 1 NURBS patch of order 2. The simulation starts with assuming the same basis functions for the approximation of the displacements as for the geometry. Refinement of the results can be achieved by order elevation or knot insertion. In the isogeometric BEM the collocation points are chosen to be the anchors of the basis functions used for the approximation of the unknown. Figure 7 shows the location of collocation points for the original and the first two stages of refinement by order elevation.

7.3 Results and Comparison

First we compare the variation of the tangential stress[1] along the tunnel surface, as a function of the number of degrees of freedom in Figure 8.

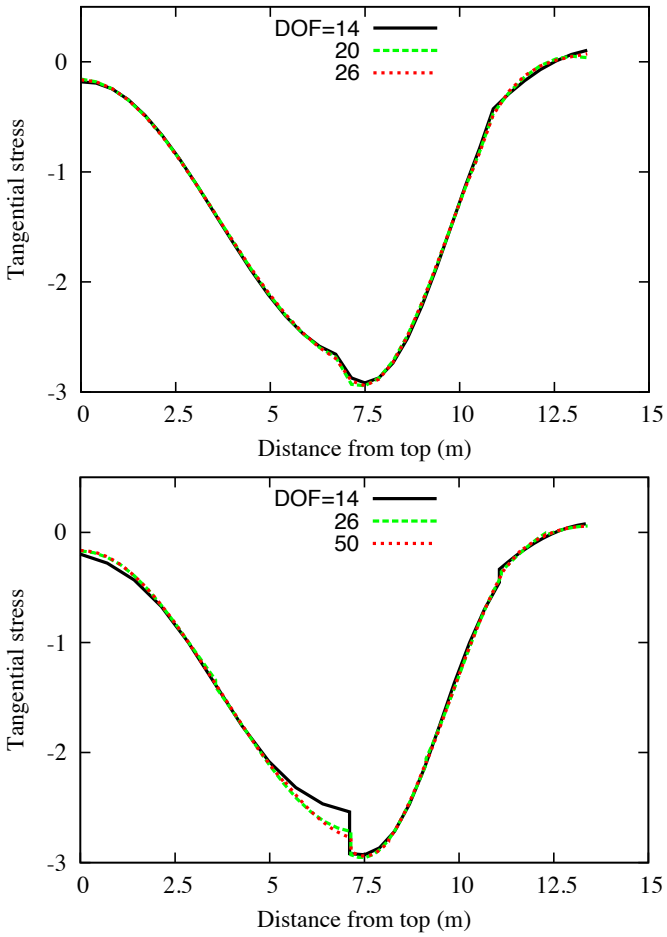

Figure 8: Distribution of tangential stress along tunnel wall for different degrees of freedom. Top: analysis with NURBS, bottom: conventional BEM analysis

It can be seen that even without refinement the NURBS based analysis gives good results, with a smooth stress distribution and very little difference between the solutions with increasing degrees of freedom. The conventional BEM analysis shows a jump in stresses between elements, which decreases as the number of degrees of freedom is increased. This is because the approximation of the geometry with isoparametric boundary elements does not have C^I continuity between elements and a small kink appears which is reduced, as the number of elements is increased. In Figure 9 we show the results of the unrefined NURBS based simulation. It can be seen that good results can be obtained with very few degrees of freedom.

8 Extension of method to include geological features

Being restricted to elastic homogeneous domains severely restricts the practical applicability of the method in geomechanics.

[1]The computation of the tangential stress using the stress recovery method is explained in [3]

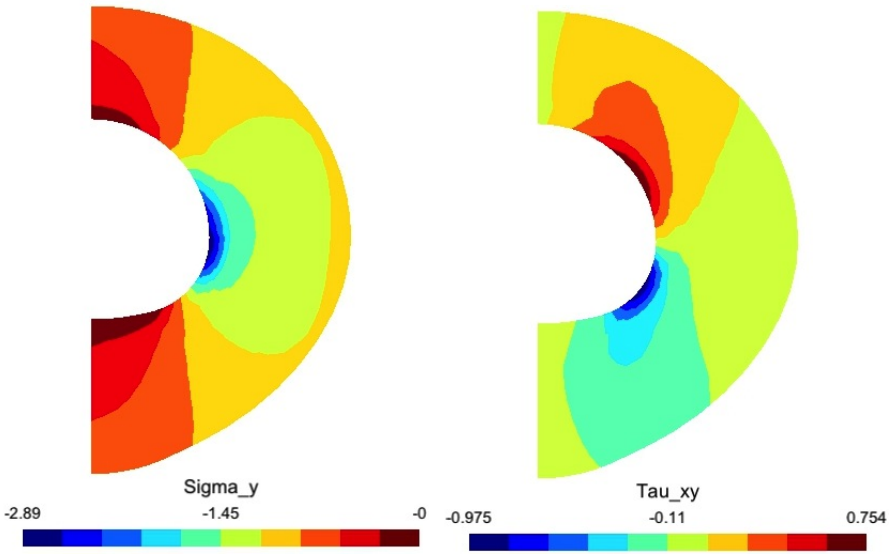

Figure 9: NATM Tunnel: Resulting stress fields

Here we extend the capabilities by considering inclusions that have different material properties and may exhibit non-linear material behavior. As mentioned earlier volume effects will appear, that have to be dealt with. The aim in the implementation will be to avoid additional discretization effort because of this.

The basic approach is to use an iterative solution method. First the problem is solved considering an elastic homogeneous domain. Then the solution is modified to account for the presence of inclusions and inelastic behavior.

The procedure is similar to the initial stress method used in Finite Element work and can be summarized as follows:

1. Solve the elastic, homogeneous problem and determine the increment of stress $\dot{\boldsymbol{\sigma}}$ inside the inclusion V_0.
2. Determine an increment in initial stress $\dot{\boldsymbol{\sigma}}_0$ due to the fact that the elastic material properties of the inclusion are different from the ones used for the fundamental solutions and/or due to the fact that the elastic limit has been exceeded.
3. Convert $\dot{\boldsymbol{\sigma}}_0$ to body force and traction increments $\dot{\mathbf{b}}_0$, $\dot{\mathbf{t}}_0$.
4. Compute new right hand side by evaluating the arising volume and surface integrals.
5. Solve for the new right hand side and compute a new increment of stress $\dot{\boldsymbol{\sigma}}$ inside the inclusion.
6. Repeat 2. to 5. until $\dot{\boldsymbol{\sigma}}_0$ is sufficiently small.

8.1 Elastic inclusions

Elastic inclusions can be modeled with the multi-region method (see for example [2]) and this involves an additional discretization and increases the number of unknowns. Here we include their treatment in the iterative process required for plasticity.

To compute the initial stress increment for the case where the inclusions have elastic properties which are different to the ones used for the fundamental solutions we use the relation between increments of stress $\dot{\boldsymbol{\sigma}}$ and strain $\dot{\boldsymbol{\epsilon}}$ in Voigt notation

$$\dot{\boldsymbol{\sigma}} = \mathbf{C}\,\dot{\boldsymbol{\epsilon}} \tag{11}$$
$$\dot{\boldsymbol{\epsilon}} = \mathbf{C}^{-1}\,\dot{\boldsymbol{\sigma}} \tag{12}$$

where $\mathbf{C}$ is the constitutive matrix for the domain used for the computation of the fundamental solutions. The difference in stress between the inclusion and the domain and therefore the initial stress increment can be computed by

$$\dot{\boldsymbol{\sigma}}_0 = (\mathbf{C}_i - \mathbf{C})\,\dot{\boldsymbol{\epsilon}} \tag{13}$$

where $\mathbf{C}_i$ is the constitutive matrix for the inclusion.

8.2 Inelastic behavior

If the inclusion experiences inelastic behavior then additional initial stresses are generated. Here we use the concept of visco-plasticity, but it is obvious that the method presented here can also be applied to elasto-plasticity. In visco-plasticity we specify a visco-plastic strain rate

$$\frac{\partial \boldsymbol{\epsilon}^{vp}}{\partial t} = \frac{1}{\eta}\Phi(F)\frac{\partial Q}{\partial \boldsymbol{\sigma}} \tag{14}$$

where η is a viscosity parameter, F is the yield function, Q the plastic potential [12]. It holds that

$$\Phi(F) = 0 \quad for \quad F < 0 \tag{15}$$
$$\Phi(F) = F \quad for \quad F > 0. \tag{16}$$

The visco-plastic strain increment during a time increment Δt can be computed by an explicit scheme

$$\dot{\boldsymbol{\epsilon}}^{vp} = \frac{\partial \boldsymbol{\epsilon}^{vp}}{\partial t}\Delta t. \tag{17}$$

The time step Δt can not be chosen freely and if chosen too large, oscillatory behavior will occur in the solution. Suitable time step values can be found in [13]. The initial stress increment is given by

$$\dot{\boldsymbol{\sigma}}_0 = \mathbf{C}\,\dot{\boldsymbol{\epsilon}}^{vp}. \tag{18}$$

8.3 Previous work

The first BEM formulation for inelastic problems has been proposed in [14]. The method has been improved substantially in [15], [16] and [17]. The latter approach proposed an initial strain formulation in which the consistent tangential operator [12] is used to obtain convergence of quadratic order for the iterative solution procedure.

The common approach for the evaluation of the necessary domain integration is to use cells which are identical to isoparametric finite elements. The cell based method for solving inelastic problems with the BEM is explained in detail in [18] and [2]. To overcome the need for a volume discretization, approaches such as the dual reciprocity BEM [19] or the use of radial basis functions [20] have been proposed. A comparison of these methods to the cell based approach found in [21] recommends the latter for accuracy and robustness. Moreover, radial basis

functions are not suitable for the analysis of infinite domains. The possibility to automatically generate cells in the inelastic region has been explored in [22]. In [23] and [24] the cell method is extended to cover the simulation of elastic inclusions with different material properties and in [25] applied to a fast BEM formulation.

All these approaches require the generation of a mesh of cells, which adds an additional effort. Therefore the main innovation presented here is that the concept of cells is abandoned and replaced by a geometry definition of the inclusion as will be explained. It is expected that this approach will not only make the simulation of these simulations more user friendly but we expect also an increase in accuracy of the results, because the approximation of initial stress inside cells with basis functions is avoided. An important aspect regarding accuracy is that most published cell based methods a continuous variation of initial stresses is assumed, regardless of the fact that the elasto-plastic boundary may cut through a cell and that in this case the variation of the initial stress is discontinuous.

In the following it is first outlined how the geometry of inclusions is defined using NURBS curves and how the arising volume and surface integrals are numerically evaluated.

9 Geometry definition for inclusions

The first task is the description of the geometry of the subdomain V_0. For this we propose to use a mapping method introduced recently for trimmed surfaces in [9] and [3]. This means that the subdomain is defined by two NURBS curves and a linear interpolation between them.

We establish a local coordinate system $\mathbf{s} = (s,t)^\intercal = [0,1]^2$ as shown in Figure 10 and perform all computations such as integration and differentiation in this system and then map it to the global x,y-system. Note that there is a one to one mapping between the coordinate $s = [0,1]$ and coordinate u of the red and green NURBS curve in Figure 10 . The global coordinates of a point $\mathbf{x}$ with the local coordinates $\mathbf{s}$ are given by

$$\mathbf{x}(s,t) = (1-t)\,\mathbf{x}^I(s) + t\,\mathbf{x}^{II}(s) \tag{19}$$

where

$$\mathbf{x}^I(s) = \sum_{k=1}^{K^I} R_k^I(s)\,\mathbf{x}_k^I \quad \text{and} \quad \mathbf{x}^{II}(s) = \sum_{k=1}^{K^{II}} R_k^{II}(s)\,\mathbf{x}_k^{II}. \tag{20}$$

The superscript I relates to the bottom (red) curve and II to the top (green) curve and $\mathbf{x}_k^I$, $\mathbf{x}_k^{II}$ are control point coordinates. K^I and K^{II} are the number of control points, $R_k^I(s)$ and $R_k^{II}(s)$ are NURBS basis functions. The derivatives are given by

$$\begin{aligned} \frac{\partial \mathbf{x}(s,t)}{\partial s} &= (1-t)\,\frac{\partial \mathbf{x}^I(s)}{\partial s} + t\,\frac{\partial \mathbf{x}^{II}(s)}{\partial s} \\ \frac{\partial \mathbf{x}(s,t)}{\partial t} &= -\mathbf{x}^I(s) + \mathbf{x}^{II}(s) \end{aligned} \tag{21}$$

where

$$\begin{aligned} \frac{\partial \mathbf{x}^I(s)}{\partial s} &= \sum_{k=1}^{K^I} \frac{\partial R_k^I(s)}{\partial s}\,\mathbf{x}_k^I \\ \frac{\partial \mathbf{x}^{II}(s)}{\partial s} &= \sum_{k=1}^{K^{II}} \frac{\partial R_k^{II}(s)}{\partial s}\,\mathbf{x}_k^{II}. \end{aligned} \tag{22}$$

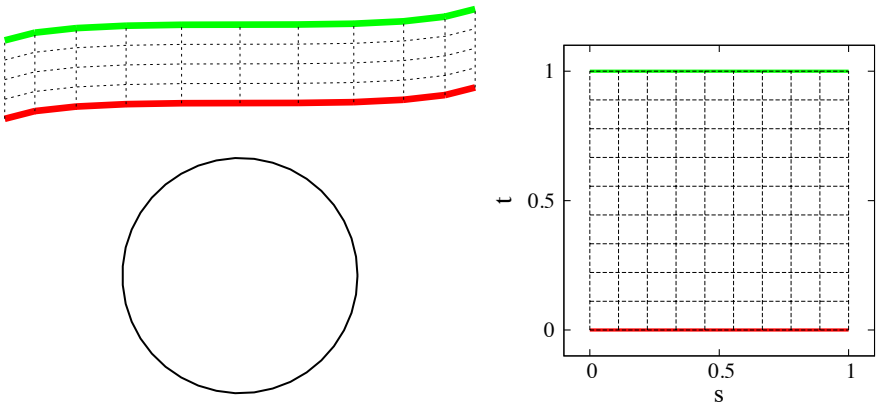

Figure 10: A circular excavation with an inclusion above it: Definition of the geometry of the inclusion with 2 NURBS curves in left global and right local coordinate space

The Jacobian matrix of this mapping is

$$\mathbf{J} = \begin{pmatrix} \frac{\partial x}{\partial s} & \frac{\partial y}{\partial s} \\ \\ \frac{\partial x}{\partial t} & \frac{\partial y}{\partial t} \end{pmatrix} \tag{23}$$

and the Jacobian is $J(\mathbf{s}) = |\mathbf{J}|$.

Remark: The geometry definition just outlined is suitable for geological inclusions of tabular shape, as are defined in the following examples. However, the theory presented is not restricted to this geometry definition and any definition that involves a mapping to a local coordinate system $\mathbf{s}$ can be used.

10 Computation of $\{\mathbf{F}\}_0$

Here we discuss the computation of the right hand side during iteration. This involves the evaluation of the integrals in Equation (2) over S_0 and V_0 of the inclusion using numerical integration (Gauss quadrature). First the initial stresses have to be converted to tractions acting on boundary S_0 and body forces acting in the domain V_0. The traction increments are given by:

$$\dot{\mathbf{t}}_0 = \begin{pmatrix} \dot{\sigma}_{0x} & \dot{\tau}_{0xy} \\ \dot{\tau}_{0xy} & \dot{\sigma}_{0y} \end{pmatrix} \mathbf{n} \tag{24}$$

where $\mathbf{n}$ is the unit outward normal vector to the surface S_0. The body force increment $\dot{\mathbf{b}}_0$ can be computed by

$$\dot{\mathbf{b}}_0 = -\begin{pmatrix} \frac{\partial \dot{\sigma}_{0x}}{\partial x} + \frac{\partial \dot{\tau}_{0xy}}{\partial y} \\ \\ \frac{\partial \dot{\tau}_{0xy}}{\partial x} + \frac{\partial \dot{\sigma}_{0x}}{\partial y} \end{pmatrix} \tag{25}$$

It is convenient to compute the derivatives with respect to local coordinates $\mathbf{s}$ first and then transform them to global coordinates. For example the global derivatives of σ_x in terms of local derivatives are given by the transformation

$$\boldsymbol{\sigma}_{x,\mathbf{x}} = \mathbf{J}^{-1}\,\boldsymbol{\sigma}_{x,\mathbf{s}} \tag{26}$$

where

$$\boldsymbol{\sigma}_{x,\mathbf{x}} = \begin{pmatrix} \frac{\partial \sigma_x}{\partial x} \\ \frac{\partial \sigma_x}{\partial y} \end{pmatrix} \quad \text{and} \quad \boldsymbol{\sigma}_{x,\mathbf{s}} = \begin{pmatrix} \frac{\partial \sigma_x}{\partial s} \\ \frac{\partial \sigma_x}{\partial t} \end{pmatrix} \tag{27}$$

and $\mathbf{J}$ is the Jacobian matrix (23).

The derivatives are numerically computed using finite differences. We define a regular grid of points inside the inclusion in the local coordinate system $\mathbf{s}$. For grid points that have other points left and right (or top and bottom) of them we use a central finite difference, whereas for points that only have one point on a side we use forward or backward finite differences.

Remark: In the following examples a simple linear interpolation between grid points and a linear extrapolation from grid points to the boundary S_0. Obviously more sophisticated schemes may be applied. However care has to be taken that the variation of the initial stress may be discontinuous. The simple scheme applied here leads to an increase in the accuracy for determination of the derivatives and for the evaluation of the associated integrals as the number of grid points is increased. The convergence of the solution as a function of the number of internal points is investigated in [26].

The numerical evaluation of $\{\mathbf{F}\}_0^{S_0}$ and $\{\mathbf{F}\}_0^{V_0}$ is explained in detail in [26].

11 Computation of results inside the inclusion

As mentioned above, the solution algorithm requires the evaluation of strains and stresses at internal points. For the initial solution (without body forces) the displacements at a point $\mathbf{y}_i$ inside the inclusion V_0 can be computed by

$$\mathbf{u}(\mathbf{y}_i) = \int_S \mathbf{U}(\mathbf{y}_i, \mathbf{x})\, \mathbf{t}(\mathbf{x})\, \mathrm{d}S - \int_S \mathbf{T}(\mathbf{y}_i, \mathbf{x})\, \mathbf{u}(\mathbf{x})\, \mathrm{d}S. \tag{28}$$

The strain at a point $\mathbf{y}_i$ inside the inclusion is

$$\boldsymbol{\epsilon}(\mathbf{y}_i) = \int_S \mathbf{S}(\mathbf{y}_i, \mathbf{x})\, \mathbf{t}(\mathbf{x})\, \mathrm{d}S - \int_S \mathbf{R}(\mathbf{y}_i, \mathbf{x})\, \mathbf{u}(\mathbf{x})\, \mathrm{d}S \tag{29}$$

where $\mathbf{S}$ and $\mathbf{R}$ are derived fundamental solutions [2]. The stresses can be computed using (11).

For the subsequent solution (including body forces) the displacements at a point $\mathbf{y}_i$ inside the inclusion is

$$\begin{aligned} \mathbf{u}(\mathbf{y}_i) = &\int_S \mathbf{U}(\mathbf{y}_i, \mathbf{x})\, \mathbf{t}(\mathbf{x})\, \mathrm{d}S - \int_S \mathbf{T}(\mathbf{y}_i, \mathbf{x})\, \mathbf{u}(\mathbf{x})\, \mathrm{d}S \\ &+ \int_{S_0} \mathbf{U}(\mathbf{y}_i, \bar{\mathbf{x}})\, \dot{\mathbf{t}}_0(\bar{\mathbf{x}})\, \mathrm{d}S_0 + \int_{V_0} \mathbf{U}(\mathbf{y}_i, \bar{\mathbf{x}})\, \dot{\mathbf{b}}_0(\bar{\mathbf{x}})\, \mathrm{d}V_0 \end{aligned} \tag{30}$$

The strain can be computed by

$$\begin{aligned} \boldsymbol{\epsilon}(\mathbf{y}_i) = &\int_S \mathbf{S}(\mathbf{y}_i, \mathbf{x})\, \mathbf{t}(\mathbf{x})\, \mathrm{d}S - \int_S \mathbf{R}(\mathbf{y}_i, \mathbf{x})\, \mathbf{u}(\mathbf{x})\, \mathrm{d}V \\ &+ \int_{S_0} \mathbf{S}(\mathbf{y}_i, \bar{\mathbf{x}})\, \dot{\mathbf{t}}_0(\bar{\mathbf{x}})\, \mathrm{d}S_0 + \int_{V_0} \mathbf{S}(\mathbf{y}_i, \bar{\mathbf{x}})\, \dot{\mathbf{b}}_0(\bar{\mathbf{x}})\, \mathrm{d}V_0 \end{aligned} \tag{31}$$

Again, for the evaluation of the integrals Gauss integration is used and is described in detail in [26].

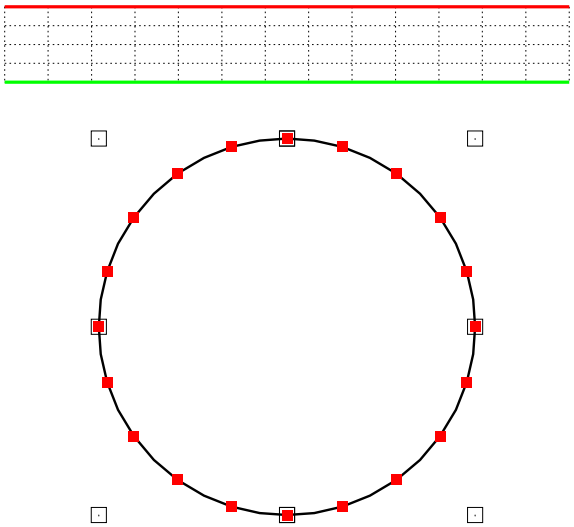

Figure 11: Test example 1: Definition of the geometry of the excavation and the inclusion with 2 NURBS curves. Control points for the excavation are shown as hollow squares, red squares indicate the collocation points used for the analysis.

12 Test examples

The theory is tested on two simple examples here and comparison is made with a coupled BEM/FEM analysis.

12.1 Example 1: Elastic inclusion above circular excavation

Here we test the capability of the method to simulate elastic inclusions. The example is that of a circular excavation in an infinite domain with the following properties:

E=1; Poissons ratio=0, virgin stress $\sigma_{x0} = 0$, $\sigma_{y0} = -1$.

Above the circular excavation there is an elastic inclusion with the elastic modulus of half the one assumed for the domain. Figure 11 shows the geometry definition of the excavation and the inclusion. The solution was achieved by order elevating the basis functions used for the description of the geometry three times. Figure 12 shows that the simulation converges after 8 iterations and that the end result compares well with a coupled Boundary/Finite element analysis using the software BEFE. The results of the simulation are shown in Figure 13.

12.2 Example 2: Elasto-plastic inclusion above circular excavation

This is the same example as the previous one except that the inclusion has the same elastic properties as the domain but has elasto-plastic properties. In this case a laminate plasticity model was applied with a horizontal orientation of the lamina and a Mohr-Coulomb yield condition. The properties assumed were:

Angle of friction $\phi : 10^\circ$, c: 0, non-associative flow law with $\psi : 0$.

The convergence of the maximum displacement after about 10 iterations is shown in Figure 14 and compared with a coupled analysis using BEFE.

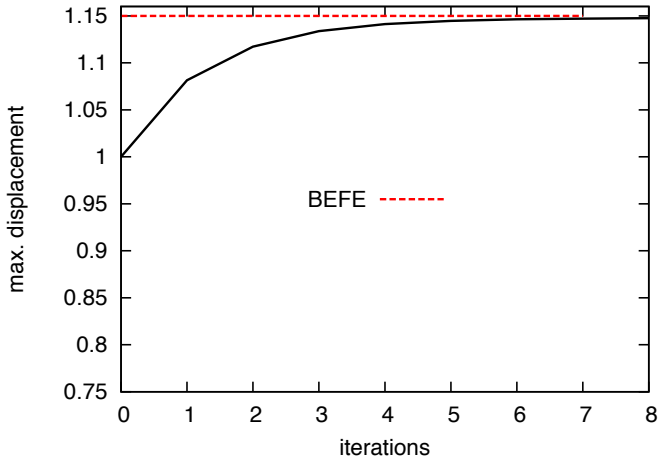

Figure 12: Convergence of maximum displacement as a function of the number of iterations

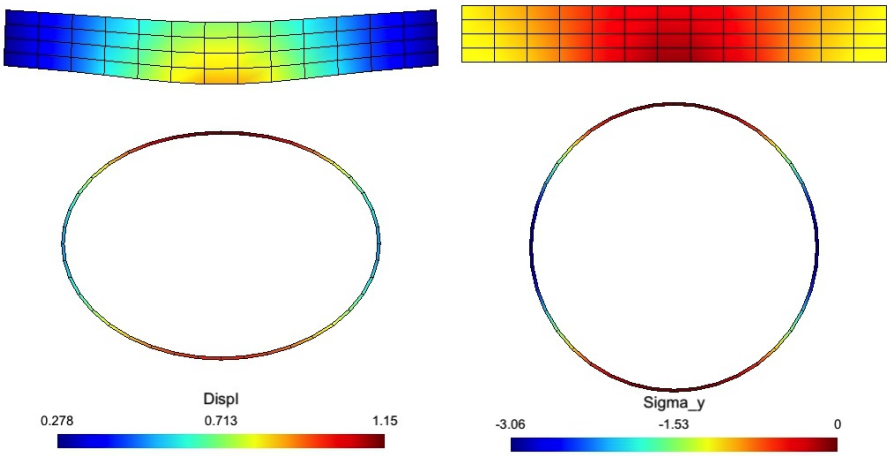

Figure 13: Results of the simulation. Left: Displaced shape; Right: Vertical stress

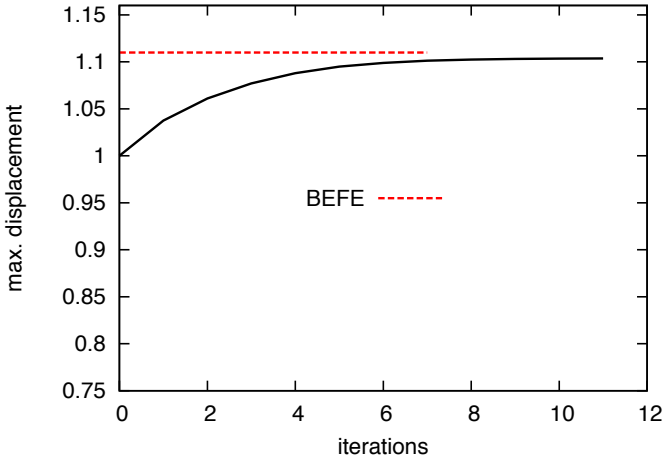

Figure 14: Example 2: Convergence of maximum displacement as a function of the number of iterations

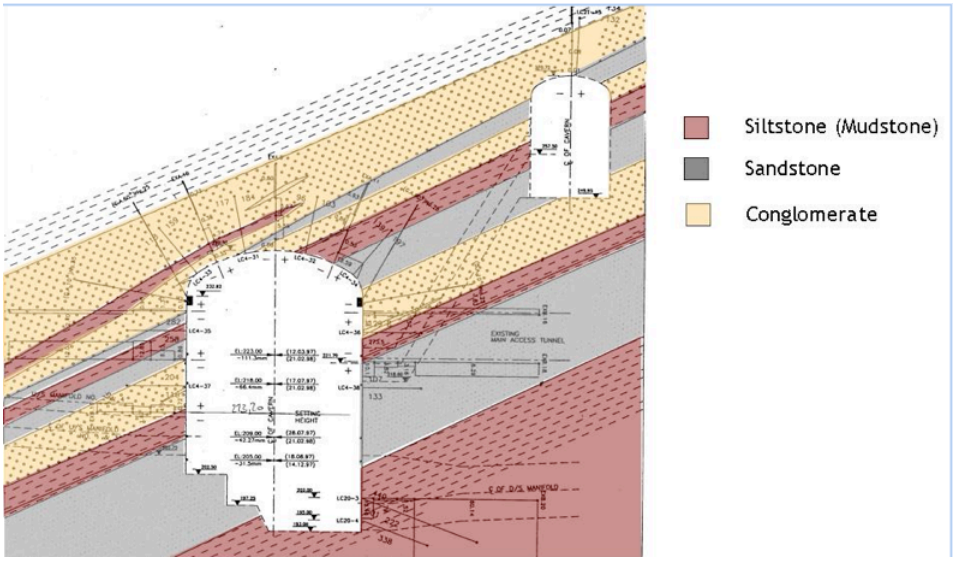

Figure 15: Practical example: Geometry of cavern showing the geology.

Rock mass	
Young's modulus	E=10000 MPa
Poisson's ratio	ν=0.20
Inclusion	
Young's modulus	E_i=6000 MPa
Poisson's ratio	ν_i=0.25
Mohr-Coulomb yield condition	
Angle of friction	ϕ=30°
Cohesion	c=0.73 MPa
Virgin stress field	σ_{xv}=−4 MPa
	σ_{yv}=−8 MPa

Table 1: Practical example: Material parameters and stress field

13 Practical example

The practical example is one that has been solved with a coupled BEM/FEM method and reported in [2]. It relates to the plane strain analysis of an underground power station cavern. Figure 15 shows a sketch of the final excavation stage together with the geology which basically consists of mudstone, sandstone and conglomerate. The mudstone is the weakest material and has the most profound effect on the ground behaviour. Therefore these layers have been modelled in the simulation reported in [2].

The material parameters assumed in the simulation are summarised in Table 1. For revisiting the coupled BEM/FEM analysis with the novel simulation method, using BEM only we consider an excavation stage to level 232 m and a limited extent of the inclusions. It should be noted here that no truncation of the mesh is necessary, as the solution obeys the radiation condition. The limited extent of the inclusions simply means that the effect of the mudstone layers diminishes at a distance from the excavation surface.

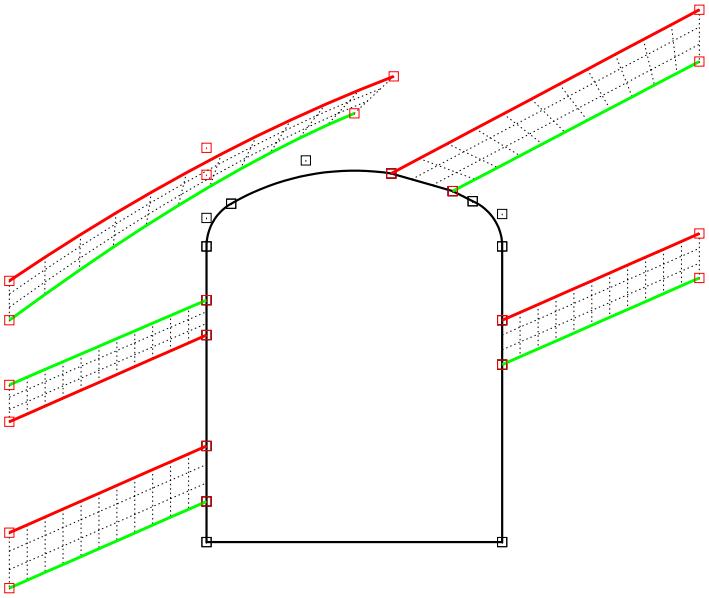

Figure 16: Practical example: The geometry of the cavern is described by 14 NURBS patches. The associated control points are shown as hollow black squares. Five inclusions are described by bounding curves with the associated control points shown as red hollow squares

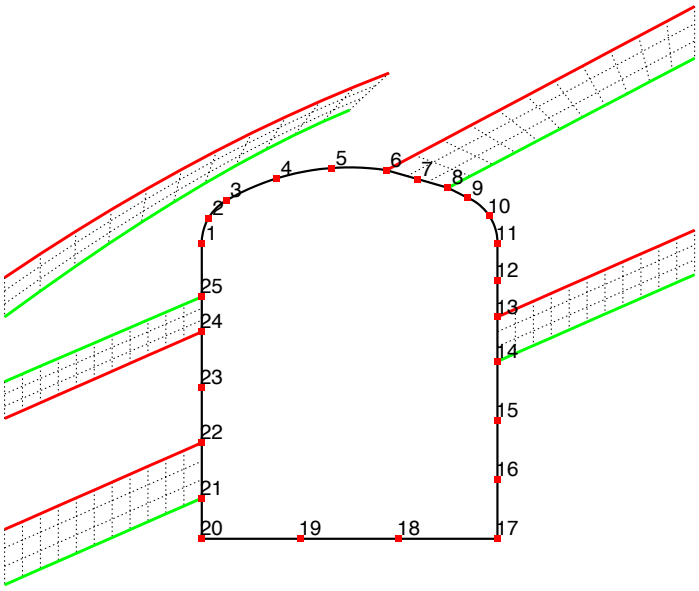

Figure 17: Practical example: Figure showing the location of collocation points

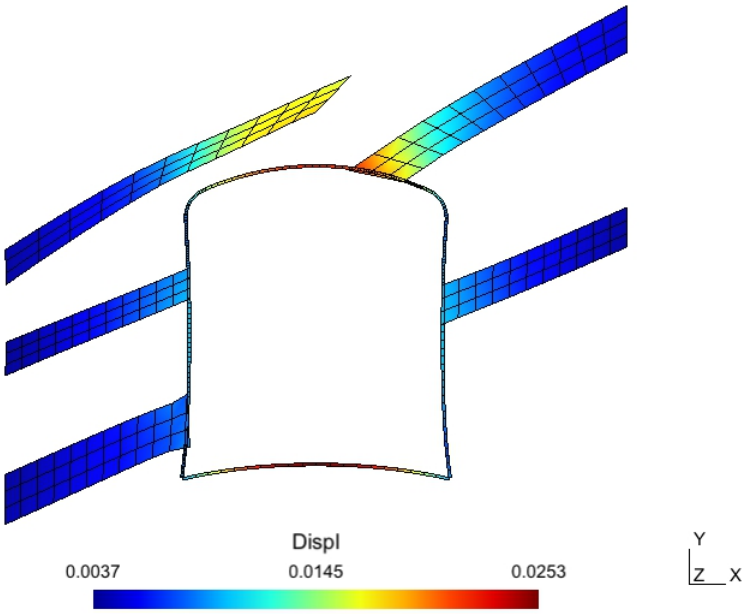

Figure 18: Practical example: Displaced shape

Figure 16 shows the geometry of the cavern with the discretization into 14 NURBS patches. For the analysis some basis functions for describing the geometry were order elevated, resulting the the collocation points shown in Figure 17. The resulting displacements are shown in Figure 18.

14 Summary and Conclusions

The aim of the paper was to show recent advances of the Boundary Element Method with applications in geomechanics. It has been demonstrated that the use of NURBS basis functions results in a significantly more efficient simulation with fewer parameters required for accurately describing the geometry and fewer degrees of freedom. It was also shown that NURBS technology can be used for the definition of geological inclusions with few parameters, resulting in more efficient simulation of these problems. The claims have been verified by test examples and a practical application. An extension of the theory to 3-D problems is underway.

REFERENCES

[1] T. Hughes, J. Cottrell, Y. Bazilevs, Isogeometric analysis: CAD, finite elements, NURBS, exact geometry and mesh refinement, Computer Methods in Applied Mechanics and Engineering 194 (39–41) (2005) 4135–4195.
URL http://www.sciencedirect.com/science/article/pii/S0045782504005171

[2] G. Beer, I. Smith, C. Duenser, The Boundary Element Method with Programming, Springer-Verlag, Wien, 2008.

[3] G. Beer, Advanced numerical simulation methods - From CAD Data directly to simulation results, CRC Press/Balkema, 2015.

[4] R. Simpson, S. Bordas, J. Trevelyan, T. Rabczuk, A two-dimensional isogeometric boundary element method for elastostatic analysis, Computer Methods in Applied Mechanics and Engineering 209–212 (0) (2012) 87–100.
URL http://www.sciencedirect.com/science/article/pii/S0045782511002635

[5] M. Scott, R. Simpson, J. Evans, S. Lipton, S. Bordas, T. Hughes, T. Sederberg, Isogeometric boundary element analysis using unstructured T-splines, Computer Methods in Applied Mechanics and Engineering 254 (0) (2013) 197 – 221. doi:10.1016/j.cma.2012.11.001.
URL http://www.sciencedirect.com/science/article/pii/S0045782512003386

[6] B. Marussig, G. Beer, C. Duenser, Isogeometric boundary element method for the simulation in tunneling, Applied Mechanics and Materials 553 (2014) 495–500.

[7] G. Beer, B. Marussig, J. Zechner, C. Duenser, T.-P. Fries, Boundary Element Analysis with trimmed NURBS and a generalized IGA approach, in: E. Oñate, J. Oliver, A. Huerta (Eds.), 11th World Congress on Computational Mechanics (WCCM XI), 2014.

[8] B. Marussig, J. Zechner, G. Beer, T.-P. Fries, Fast isogeometric boundary element method based on independent field approximation, Computer Methods in Applied Mechanics and Engineering 284 (0) (2015) 458 – 488, isogeometric Analysis Special Issue.

[9] G. Beer, B.Marussig, J. Zechner, A simple approach to the numerical simulation with trimmed CAD surfaces, Computer Methods in Applied Mechanics and Engineering 285 (2015) 776–790.

[10] G. Beer, Mapped infinite patches for the NURBS based boundary element analysis in geomechanics, Computers and Geotechnics 66 (2015) 66–74.

[11] G. Beer, S. Bordas (Eds.), Isogeometric methods for numerical simulation, CISM lecture notes, Springer, 2014.

[12] J. Simo, T. Hughes, Computational Inelasticity, Springer, 1998.

[13] I. Cormeau, Numerical stability in quasi-static elasto-viscoplasticity, International Journal for Numerical Methods in Engineering 9 (1).

[14] J. Swedlow, T. Cruse, Formulation of boundary integral equations for three-dimensional elasto-plastic flow, International Journal of Solids and Structures 7 (12) (1971) 1673 – 1683. doi:10.1016/0020-7683(71)90006-0.
URL http://www.sciencedirect.com/science/article/pii/0020768371900060

[15] J. C. F. Telles, C. A. Brebbia, On the application of the boundary element method to plasticity, Applied Mathematical Modelling 3 (1979) 466–470.

[16] J. C. F. Telles, J. A. M. Carrer, Implicit procedures for the solution of elastoplastic problems by the boundary element method, Mathematical and Computer Modelling 15 (1991) 303–311.

[17] M. Bonnet, S. Mukherjee, Implicit bem formulations for usual and sensitivity problems in elasto-plasticity using consistent tangent operator concept, International Journal of Solids and Structures 33 (30) (1996) 4461–4480.

[18] X.-W. Gao, T. G. Davies, Boundary Element Programming in Mechanics, Cambridge University Press, Cambridge, 2002.

[19] D. P. Henry, P. K. Banerjee, A new bem formulation for two- and three-dimensional elastoplasticity using particular integrals, International Journal for Numerical Methods in Engineering 26 (9) (1988) 2079–2096. doi:10.1002/nme.1620260912.
URL http://dx.doi.org/10.1002/nme.1620260912

[20] X.-W. Gao, A boundary element method without internal cells for two-dimensional and three-dimensional elastoplastic problems, Journal of Applied Mechanics 69 (2) (2002) 154–160. doi:10.1115/1.1433478.
URL http://link.aip.org/link/?AMJ/69/154/1

[21] M. Ingber, A. Mammoli, M. Brown, A comparison of domain integral evaluation techniques for boundary element methods, International Journal for Numerical Methods in Engineering 52 (2001) 417–432.

[22] T. Ribeiro, G. Beer, C. Duenser, Efficient elastoplastic analysis with the boundary element method, Computational Mechanics 41 (2008) 715–732.
URL http://dx.doi.org/10.1007/s00466-007-0227-1

[23] K. Riederer, C. Duenser, G. Beer, Simulation of linear inclusions with the BEM, Engineering Analysis with Boundary Elements 33 (7) (2009) 959 – 965. doi:10.1016/j.enganabound.2009.01.003.
URL http://www.sciencedirect.com/science/article/pii/S0955799709000125

[24] K. Riederer, Modelling of Ground Support in Tunnelling using the BEM, Ph.D. thesis, Graz University of Technology (2010).

[25] J. Zechner, G. Beer, A fast elasto-plastic formulation with hierarchical matrices and the boundary element method, Computational Mechanics 51 (4) (2013) 443–453.

[26] G. Beer, B. Marussig, J. Zechner, C. Duenser, T. P. Fries, Isogeometric boundary element analysis with elasto-plastic inclusions. part 1: plane problems, Computer Methods in Applied Mechanics and Engineering.